Original Research

Eco-Friendly Synthesis of Zinc Oxide Nanoparticles Using *Withania Coagulans* Fruit Extract: Characterization, Antioxidant Activity and Photocatalytic Potential

M. Iqbal[1,2], M. M. Akbar[3], N. Alwadai[4,*], N. Ahmad[3], M. Abbas[5], I. Bibi[6], A.H. Almuqrin[4], N. Tamam[4], M.S. Alshatwi[4], A. Nazir[7]

[1] Renewable Energy and Environmental Technology Center, University of Tabuk, Tabuk, 47913, Saudi Arabia;
[2] School of Chemistry, University of the Punjab, Lahore, 54590, Pakistan;
[3] Department of Chemistry, Division of Science and Technology, University of Education, Lahore 54770, Pakistan;
[4] Department of Physics, College of Sciences, Princess Nourah bint Abdulrahman University, P.O. Box 84428, Riyadh 11671, Saudi Arabia;
[5] Department of Biochemistry, University of Veterinary and Animal Sciences, Lahore (Jhang-campus), Jhang 35200, Pakistan;
[6] Institute of Chemistry, The Islamia University of Bahawalpur, Bahawalpur, Pakistan;
[7] Department of Chemistry, The University of Lahore, Pakistan.
***** Correspondence: nmalwadai@pnu.edu.sa

Abstract: *Withania coagulans* fruit extract was used as a reducing and stabilizing agent in an eco-friendly synthesis process to prepare zinc oxide nanoparticles (NPs). Fourier transform infrared (FTIR) spectroscopy, X-ray diffraction, scanning electron microscopy and ultraviolet–visible spectroscopy were used to characterize the NPs. The X-ray diffraction patterns revealed a crystalline hexagonal wurtzite phase with an estimated average crystallite size of approximately 9.25 nm. The presence of a unique absorption peak at 365 nm confirmed the formation of ZnO NPs. The morphological analysis showed unevenly shaped particles with aggregates of the NPs due to the presence of biomolecules on the surface. Effective bio-capping was confirmed by the FTIR analysis, which also showed Zn–O vibrational band at 582 cm^{-1} and revealed the presence of phytochemical moieties from the extract on the NPs surface. Total phenolic content (TPC), total flavonoid content (TFC), linoleic acid oxidation inhibition and DPPH radical scavenging techniques were used to evaluate the antioxidant activity (AOA). Aqueous ethanol extracts showed a promising AOA and the highest concentrations of phenolics and flavonoids among the investigated solvents. Phenol red dye was used to evaluate the photocatalytic activity of the synthesized ZnO NPs under solar light radiation and a 90% degradation was observed in 240 minutes. This work highlights the potential uses of ZnO NPs in environmental remediation and associated biomedical disciplines by demonstrating an environmentally benign method for preparing the ZnO NPs with a significant AOA and photocatalytic efficiency.

Keywords: *Withania coagulans;* zinc oxide nanoparticles; green synthesis; antioxidant activity; photocatalytic degradation

1. Introduction

Nanotechnology has gained significant attention due to its extensive application in different fields, including biosensors, catalysts and biomedical applications [1-2]. Currently, a lot of research is dedicated to the design, development and characterization of materials ranging from 1 to 100 nanometers, encompassing the study of these materials at atomic and molecular levels [3]. Nanomaterials, when reduced to a nano-crystalline size, can exhibit atom-like behaviors. This is due to their increased surface energy, resulting from a greater surface area and a wider band gap [4]. These NPs are intriguing because they exhibit significantly different chemical and physical aspects compared to their macroscopic counterparts. This makes them particularly attractive for use in a variety of fields, including medicine, food, cosmetics, agriculture, wastewater treatment and dye degradation [5-10].

Among synthesis approaches, i.e., physical and chemical, are expensive and require hazardous chemicals and specialized equipment [2]. Green synthesis techniques, on the other hand, produce NPs that are economical, non-toxic and environmentally benign [5]. However, one of the most sustainable and benign routes for preparing metal and metal oxide NPs is green synthesis, which uses plant materials. This method has shown great promise by using renewable biological resources like plant extracts, which function as capping, stabilizing and reducing agents all at once. This technique does away with the need for hazardous chemicals and difficult reaction conditions. Plant-mediated green synthesis makes it possible to produce stable, large-scale NPs with controlled size and shape due to its ease of use, affordability, scalability and environmental friendliness. Furthermore, this method is especially appealing for applications in environmental remediation, catalysis and biomedical fields because the phytochemicals found in plant extracts improve NP stability and frequently impart additional functional properties [11]. Green synthesis is very successful in regulating the size, shape and morphology of the desired NPs in addition to helping the environmental ecosystem. The various phytochemicals found in plant extracts, including proteins, alkaloids, flavonoids, and phenolics, are essential for controlling the nucleation and growth processes, which improve the stability and homogeneity of NPs. Green synthesis is a dependable and adjustable method for creating NPs suited to particular uses because of this intrinsic control over NP characteristics, which improves their physicochemical qualities and performance [12, 13].

Zinc oxide has attracted considerable commercial and industrial interest owing to its unique physicochemical properties, which enable its application across diverse sectors, including food, feed, aerospace, healthcare, and cosmetics. These wide-ranging applications necessitate the development of environmentally safe and green synthesis methods [14]. The photocatalytic efficiency of a catalyst is closely related to its porosity, surface area, band gap energy, crystal structure, and surface hydroxyl group density [15]. ZnO NPs possess a band gap energy of approximately 3.37 eV [16], making them a promising material for the remediation of contaminants from wastewater [17].

The textile industry consumes a large amount of water during its dyeing processes, which leads to the discharge of dye-laden effluents and severe pollution of natural water bodies [18]. Such contaminated wastewater poses serious risks to human health and adversely affects aquatic ecosystems by reducing light penetration and inhibiting the growth and photosynthetic activity of aquatic plants. The development of sophisticated and effective wastewater treatment technology has improved significantly during the last 20 years. Among these, nanotechnology has become a potent and cutting-edge strategy that uses NPs with improved physicochemical characteristics for wastewater treatment and associated environmental applications [19–20]. In particular, zinc oxide NPs have gained considerable attention as photocatalysts due to their suitable band gap, high surface reactivity, and strong oxidative potential.

Under light irradiation, ZnO NPs generate reactive oxygen species that effectively degrade organic dyes and toxic pollutants into less harmful products, highlighting their strong potential for photocatalytic wastewater remediation.

The Paneer dodi (*W. coagulans*) belongs to the family *Solanaceae*. It is a small shrub commonly found in Afghanistan, Iran, Pakistan and India [21]. Plants and herbs have been reported to possess different phytochemicals, which are required to cure a variety of health disorders [22]. Besides their medicinal impact, some compounds in plant-derived extract can exhibit the properties of allelochemicals when a suitable concentration is present in the soil to affect plants grown [21]. Plant materials contain bioactive molecules that can act as synthesis and reducing agents in the fabrication of NPs, i.e., steroidal lactones (withanolides), phenolic compounds, flavonoids, alkaloids, saponins, tannins, carbohydrates, reducing sugars and organic acids. It shows promising antioxidant and anti-microbial properties [23]. These characteristics make it suitable for diverse applications [24-25]. Numerous plant-mediated routes have been employed for the synthesis of ZnO NPs with varying particle sizes and photocatalytic efficiencies, largely governed by extract composition and synthesis conditions (Table 1). Compared with previously reported systems, the *W. coagulans* can potentially be used for the preparation of ZnO NPs, which simultaneously demonstrate strong antioxidant potential and photocatalytic activity. This combined antioxidant–photocatalytic evaluation highlights the advancement of the current study over existing reports that typically focus on photocatalysis or bioactivity alone.

Based on the aforementioned facts, this work reports the use of *W. coagulans* fruit extract for the preparation of ZnO NPs, to develop. The goals were to prepare ZnO NPs using the eco-friendly approach and characterized by employing XRD, SEM, FTIR and UV–visible techniques to examine the structural, morphological and functional properties. Additionally, TPC, TFC, linoleic acid peroxidation inhibition and DPPH scavenging assays were employed to assess the antioxidant potential. The photocatalytic performance of ZnO NPs toward dye degradation under sunlight irradiation was also assessed, with the broader objective of exploring their potential applications in environmental remediation.

2. Experimental

2.1. Reagents and chemicals

The chemicals used were of analytical grade and were purchased from Sigma-Aldrich. Methanol (≥99.8%), ethanol (≥99.9%), butylated hydroxytoluene (≥99.0%), gallic acid (≥98.0%), potassium ferricyanide (≥99.0%), ammonium thiocyanate (≥99.0%), ferrous chloride (≥98.0%), ferric chloride (≥97.0%), sodium carbonate (≥99.5%), sodium hydroxide (≥98.0%), sodium nitrite (≥99.0%), trichloroacetic acid (≥99.0%), aluminum chloride (≥99.0%), ascorbic acid (≥99.0%), DPPH (≥95.0%), and zinc acetate dihydrate (≥99.0%) were used without further purification.

2.2. Preparation of extract

The *W. coagulans* fruit was collected from the Faisalabad local market. Using a grinder, the dried fruit was ground to a fine powder. Then, 100 mL of distilled water and 10 g of fruit powder were placed in an orbital shaker at 120 rpm for 6 hours at 25 °C. Other solvents and concentrations, such as ethanol and methanol, were also used to prepare the extract. After that, the extract solution was subjected to microwave for 3.5 minutes. To get rid of the residues, the extract was filtered using filter paper. A concentrated extract was obtained by employing a rotary evaporator to remove excess solvent. For additional investigation, the crude concentrated extract was kept at -4 °C [26–28].

2.3. Synthesis of ZnO-NPs

Zinc acetate dihydrate (1.5 g) was mixed with 36 mL of distilled water and mixed thoroughly [29]. After that, 16 mL of fresh *W. Coagulans* fruit extract was added to the above solution. The solution was stirred by a magnetic stirrer for 6 hours at 400 rpm and 60 ℃. After 6 hours, 1 M NaOH was mixed with

the solution, which was then stirred overnight. The precipitates were formed and NPs formation was confirmed by the change in color of the mixture. The precipitates were centrifuged (HERMLE, D-78564, Germany) at 8,000 rpm for 5 min. The NPs were washed 5 times with distilled water and then with ethanol. The recovered NPs were heated in an incubator at 100 ℃ for 4 hours, which was then ground to a fine powder using a pestle and mortar and stored for characterization.

2.4. Characterization of ZnO-NPs

Using a Shimadzu UV-2450 spectrophotometer, ultraviolet–visible absorption spectra in the 300–500 nm range were recorded to validate the formation of ZnO NPs. Scanning electron microscopy was used to analyze the surface morphology (Hitachi SX-650, Tokyo, Japan). X-ray diffraction was used to determine the crystalline structure and crystallite size of the NPs (D8 Advance, Bruker, Germany). Zn–O bonding was confirmed and surface functional groups were identified using FTIR spectroscopy (ATR Summit Lite, Thermo Scientific, USA).

2.5. Photocatalytic dye degradation

The ZnO NPs' photoatalytic activity was evaluated using the phenol red dye. To attain an adsorption equilibrium on the catalyst's surface, 10 mg of ZnO NPs were added to 20 mL of dye and the mixture was shaken in an orbital shaker for 30 minutes in the absence of light (dark). Similarly, the catalyst and dye mixture was subjected to sunlight to evaluate the ZnO NPs' photocatalytic activity (the average light intensity for the irradiation period was 1.57 × 10−4 E s−1). After a stipulated time interval, 2 mL of the solution was taken, filtered using a Millipore filter syringe and the absorbance at 570 nm was measured. Equation 1 was used to calculate the degradation efficiency [17]. An overview of the eco-friendly synthesis of ZnO NPs, their characterization and applications is depicted in Figure 1.

$$\text{Degradation (\%)} = \frac{C_0 - C_t}{C_0} \times 100 \qquad (1)$$

Where the absorbance values at time "t" before and after irradiation are referred to as C_0 and C_t, respectively.

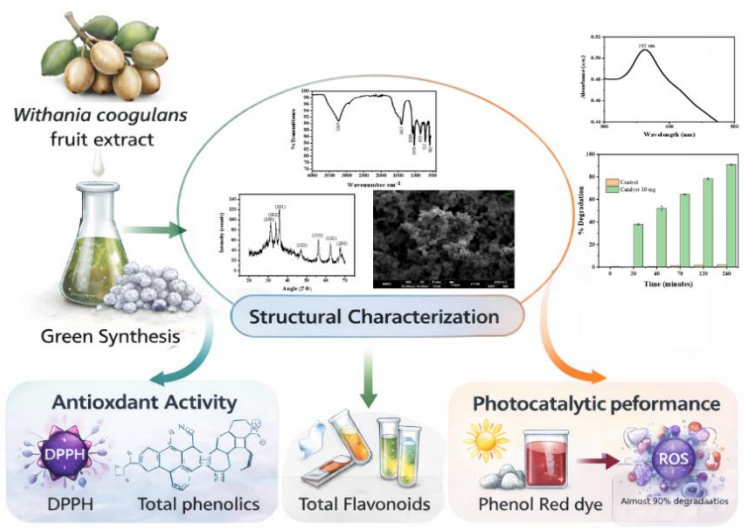

Figure 1. The schematic for the eco-friendly synthesis of ZnO NPs, characterization and applications.

2.6. Antioxidant activity

2.6.1. Evaluation of TPC

The method described by [30] was used to determine the TPC. For this, 0.5 mL of Folin-Ciocalteu reagent, 7.5 mL of distilled water and 1.5 mL of 2.5% Na_2CO_3 were mixed with 1 mg/mL of concentrated crude extract (CCE). The final solution was heated in a water bath for 25 minutes at 50 °C. At 755 nm, the resulting solution's absorbance was measured. Similar procedures were used to prepare the standard gallic acid solution (5 to 100 ppm). Gallic acid equivalent GAE/g of DW was used to calculate and express TPC. Triplicates of each of the CCE were tested for each parameter.

2.6.2. Evaluation of TFC

The method described by [28] was employed for the TFC analysis, which was estimated by dissolving 100 mg/mL of CCEs in 5 mL of distilled water and mixing 0.3 mL of 5% $NaNO_2$ in a volumetric flask. 2 mL of NaOH and 0.6 mL of 10% $AlCl_3$ were added to the resulting solution after it had been incubated for 5 minutes at room temperature. At 510 nm, the solution's absorbance was measured. Catechin equivalents (CE/g) of DW were used to calculate and express the amount of TFC. Each test was run thrice and the average of the responses was calculated.

2.6.3. Antioxidant capacity using the linoleic acid system

By preventing the oxidation of linoleic acid, the antioxidant CCEs were evaluated (28). A mixture of ethyl alcohol (10 mL; 98.8%), linoleic acid (0.13 mL), and sodium phosphate buffer (0.2 M; pH 7.1) (10 mL) was put into a 30 mL test tube. The buffer was used to dissolve a 5 mg pre-dried extract. Distilled water was added to get the volume down to 25 mL, and the mixture was then heated to 40 °C. Next, a 0.2 mL sample solution was combined with 10 mL of ethyl alcohol, 0.2 mL of aqueous ammonium thiocyanate (30%), and 20 mM of 3.5% HCl $FeCl_2$ solution. A spectrophotometer was used to measure the mixture absorbance at 500 nm. Along with standard controls such as BHT and ascorbic acid (200 ppm), fruit samples were evaluated, while linoleic acid was included in the control treatment but not in the fruit extracts. The highest peroxidation value, indicating oxidation in the absence of antioxidant molecules, was observed after 17 days in the control system. The percentage inhibition of linoleic acid peroxidation was calculated using Equation 2.

$$\text{Inhibition (\%)} = \frac{A_b - A_s}{A_b} \times 100 \qquad (2)$$

2.6.4. DPPH radical scavenging analysis

For the DPPH assay, varying concentrations of the extract (0.5–3.0 mg/mL) were mixed with 3 mL of a 0.004% methanolic DPPH solution and incubated for 20 minutes. After incubation, each sample's absorbance was measured at 517 nm and equation 3 was used to determine the radical scavenging activity (31).

$$I(\%) = 100 \times \left(\frac{A_b}{A_s}\right) \qquad (3)$$

Where "I" represents inhibition while "A_s" and "A_b" correspond to the absorbance values of the sample and blank, respectively.

3. Results and discussion

3.1. Properties of the ZnO NPs

3.1.1. UV-Vis spectroscopy

The UV–visible spectroscopy is used to analyze the optical characteristics of the ZnO NPs. The ZnO NPs prepared using *W. coagulans* fruit extract have a distinct absorption band at about 365 nm (Figure 2). This is typical of ZnO's intrinsic band-gap absorption, which results from electron transitions from the valence band to the conduction band. The appearance of a single, sharp absorption peak without

additional shoulders or secondary bands indicates the formation of phase-pure ZnO NPs and the absence of impurity-related species. Moreover, the slight broadening of the absorption edge can be attributed to nanoscale effects and size distribution of the particles, which is commonly observed in green-synthesized ZnO NPs. The observed absorption behavior is in good agreement with previously reported green route, further confirming the successful formation of ZnO nanostructures using *W. coagulans* extract [10].

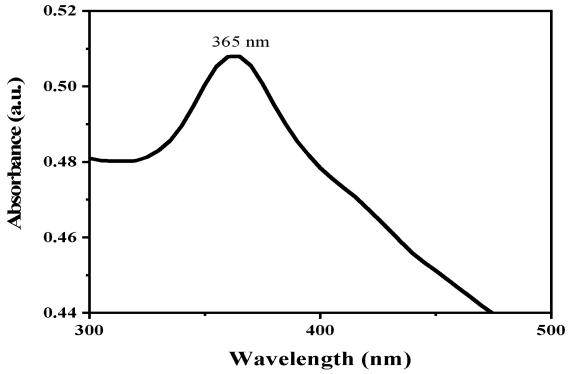

Figure 2. UV–visible spectrum of ZnO NPs prepared using *W. coagulans* fruit extract, showing a characteristic absorption peak at 365 nm.

3.1.2. Structural analysis

The green-synthesised ZnO NPs XRD pattern, recorded over a 2θ range of 20°–80°, is shown in Figure 3. The (100), (002), (101), (102), (110), (103), and (200) crystallographic planes are associated with the diffraction peaks that appear at roughly 31.7°, 34.4°, 36.2°, 47.5°, 56.6°, 62.9°, and 67.9°, respectively. The formation of single-phase ZnO with a hexagonal wurtzite crystal structure and space group $P6_3mc$ is confirmed by these reflections, which agree well with the standard JCPDS card No. 79-0208. The high phase purity of the produced NPs was demonstrated by the absence of any additional impurity-related peaks. The ZnO NPs' good crystallinity is demonstrated by the distinct and sharp diffraction peaks. The Debye–Scherrer equation (Equation 4) was used to estimate the average crystallite size.

$$D = \frac{0.9\lambda}{\beta\cos\theta} \qquad (4)$$

where θ is the Bragg angle, β is the FWHM of the strongest diffraction peak, and λ is the X-ray wavelength (1.5406 Å). The average crystallite size of the ZnO NPs was determined to be 9.25 nm. These findings support the successful synthesis and crystalline nature of the material by being in line with previously reported values for green-synthesised ZnO NPs [32].

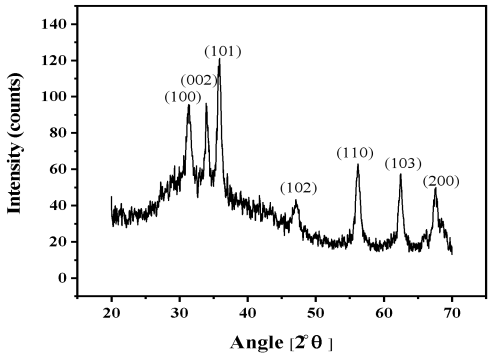

Figure 3. XRD pattern of ZnO NPs prepared using *W. coagulans* fruit extract.

3.1.3. Surface morphology

Figure 4 shows the SEM images of the ZnO NPs at different magnifications. The micrographs reveal that the ZnO NPs do not exist as well-isolated individual particles; instead, they exhibit a densely packed, agglomerated morphology forming cluster- or composite-like structures. This type of morphology is commonly reported for ZnO NPs synthesized via green or aqueous routes and is mainly attributed to the high surface energy and strong interparticle interactions of nanosized ZnO, which promote particle–particle adhesion to minimize surface free energy. The observed aggregation can also be associated with the presence of phytochemical constituents from the plant extract used during synthesis, which act as reducing and capping agents. These biomolecules may bridge adjacent NPs through hydrogen bonding or van der Waals interactions, leading to the formation of interconnected agglomerates rather than discrete particles. Similar aggregated and quasi-porous ZnO morphologies have been widely reported in literature for biogenically synthesized ZnO NPs and are considered typical for green synthesis methods [33]. Despite aggregation, the SEM images indicate a relatively homogeneous distribution of nanosized domains throughout the matrix, suggesting uniform nucleation and growth during synthesis. Such aggregated architectures are often advantageous for catalytic and photocatalytic applications, as they provide a high surface area with interconnected pathways that facilitate mass transfer and active site accessibility.

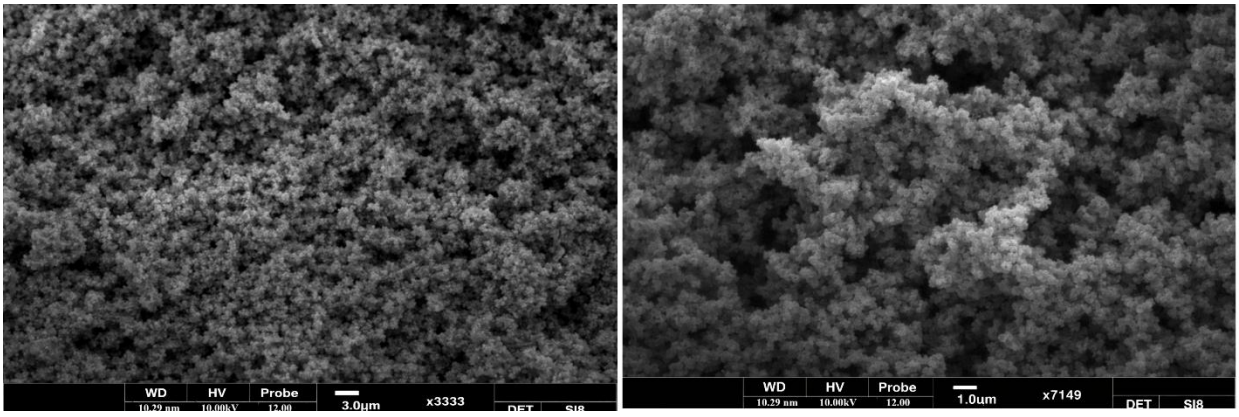

Figure 4. SEM micrographs of ZnO NPs prepared using *W. coagulans* fruit extract at different magnifications.

3.1.4. FTIR analysis

The vibrational characteristics and surface functional groups of the ZnO NPs were analyzed in the 400–4000 cm^{-1} range and the response is depicted in Figure 5. The FTIR spectrum displayed a broad absorption band around 3269 cm^{-1}, attributed to O–H stretching vibrations associated with zinc-coordinated hydroxyl groups. An absorption peak observed at 1417 cm^{-1} corresponds to symmetric stretching of carbonyl groups originating from proteinaceous components, while the band near 1034 cm^{-1} is assigned to C–N stretching vibrations of amine functionalities. A characteristic peak appearing at approximately 582 cm^{-1} confirms Zn–O lattice vibrations, verifying the successful formation of ZnO NPs [34].

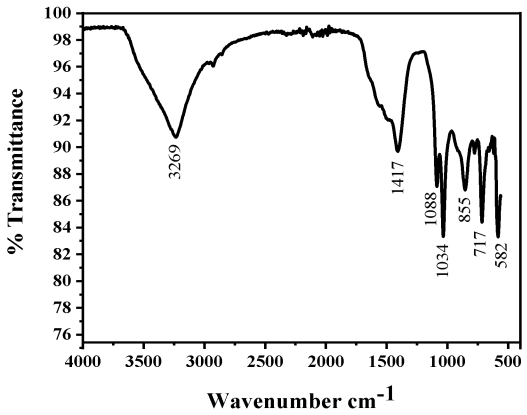

Figure 5. FTIR analysis of ZnO NPs synthesized using *W. coagulans* fruit extract.

3.2. Mechanism of ZnO NPs formation

The phytochemical-mediated complexation, hydrolysis and subsequent thermal decomposition mechanisms can account for the biosynthesis of ZnO NPs using *W. coagulans* fruit extract. The fruit extract includes bioactive components with hydroxyl, carbonyl and carboxyl functional groups, including phenolics, flavonoids, alkaloids, tannins and reducing sugars. During the formation of NPs, these functional groups serve as both stabilizing and chelating agents [19-20]. Initially, zinc precursor ions (Zn^{2+}) interact with oxygen-donor functional groups of phytochemicals present in the extract, leading to the formation of intermediate Zn–biomolecule complexes. This coordination step stabilizes Zn^{2+} in solution and controls nucleation. A similar metal–phytochemical chelation mechanism has been described for biosynthesized CuO nano-platelets, where plant metabolites facilitate controlled growth through surface binding and complex formation. The complexation is represented in Equation 5, while upon adjustment of pH or heating, hydrolysis of the zinc complex occurs, forming zinc hydroxide intermediates (Equation 6). The subsequent dehydration during thermal treatment or drying converts zinc hydroxide into crystalline ZnO NPs (Equation 7) [19-20].

$$Zn^{2+} + \text{phytochemicals} \rightarrow [Zn - \text{phytochemicals}]^{2+}\text{complex} \quad (5)$$

$$[Zn - \text{phytochemicals}]^{2+}\text{complex} + OH^{-} \rightarrow Zn(OH)_2 + \text{phytochemical residues} \quad (6)$$

$$Zn(OH)_2 \rightarrow ZnO + H_2O \quad (7)$$

This mechanism is consistent with the method described for the biogenic fabrication of ZnO NPs using saffron extract, in which ZnO is first nucleated and grown through hydroxide intermediates after

phytochemicals first coordinate Zn^{2+} ions [19–20]. Additionally, the biomolecules adsorbed on the surface of the NPs serve as capping agents, limiting excessive development and partially regulating particle size. The overall biosynthesis mechanism involves: (i) chelation of Zn^{2+} ions by phytochemicals, (ii) formation of $Zn(OH)_2$ nuclei through hydrolysis, (iii) dehydration to ZnO under thermal conditions and (iv) stabilization of the formed NPs by surface-bound organic residues. This synergistic action of reduction, complexation and stabilization by natural metabolites confirms the crucial role of *W. coagulans* extract as an effective bio-chelating and structure-directing agent in the formation of wurtzite ZnO NPs.

3.3. Photocatalytic activity

ZnO NPs showed an excellent photocatalytic response and phenol red dye was removed from the sample under irradiation in the presence of ZnO catalyst. For the irradiation times of 20, 40, 70, 120 and 240 (min), the dye removal was measured to be 0, 37, 52, 64, 78 and 90% as depicted in Fig. 6. The increased dye degradation is linked to the generation of highly reactive species like $^{\bullet}OH$ radical, which are produced when ZnO NPs are exposed to light and resultantly, the reactive species are produced. Excitement of electrons from valence into the conduction band forms an e^- and h^+ pair under irradiation. When e^- (conduction band) combines with oxygen, it produces superoxide radical. When h^+ reacts with water, it produces $^{\bullet}OH$ radical. The dye molecule is oxidatively degraded into less harmful and lower molecular weight intermediates and ultimately H_2O, CO_2 and inorganic ions. The photocatalytic activity of ZnO NPs showed that phenol red dye may be removed economically by visible light exposure. The ZnO NPs particle size has a promising impact on the photocatalytic efficacy, as smaller crystallite sizes generally provide higher surface area, more active sites, and reduced charge carrier recombination. In green-synthesized systems, controlled optimization of synthesis parameters significantly influences particle size and, consequently, environmental performance. For instance, Adraoui et al. [17] demonstrated that optimizing plant mass, precursor concentration and calcination temperature via Box–Behnken Design led to ZnO NPs with enhanced photodegradation efficiency toward Orange G dye under sunlight irradiation. In this context, further investigation of the size-dependent photocatalytic activity of the present *W. coagulans*-mediated ZnO NPs would provide deeper insight into their environmental application potential.

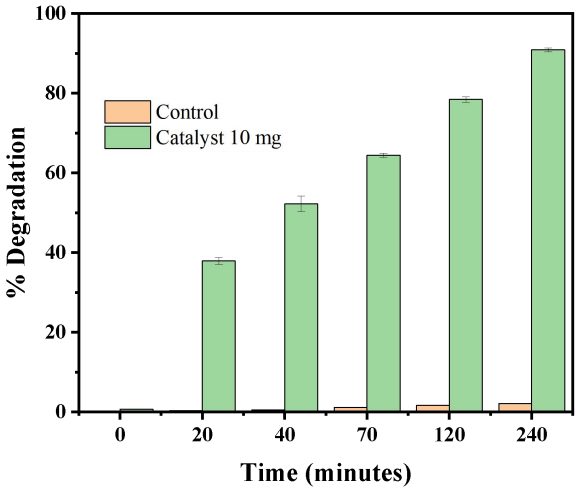

Figure 6. Photocatalytic degradation of dye using ZnO NPs under light irradiation.

3.4. Antioxidant activity

3.4.1. Percentage yield of crude extract

Aqueous methanol, pure ethanol, aqueous ethanol (80%) and distilled water were the solvents in which the yield of *W. coagulans* extract, expressed in grams per 100 grams, which revealed a variable trend. Aqueous ethanol yielded the highest percentage (10.2%), whereas distilled water yielded the lowest (6.02%) yield (Table 2). Aqueous ethanol > aqueous methanol > absolute ethanol > absolute methanol > distilled water was the order of extraction efficiency for *W. coagulans* fruit across solvents. Notably, aqueous ethanol produced the highest yield, indicating that it has a better ability to extract phytochemicals from the sample. Notable differences (p <0.05) were found using statistical analysis among solvents, with ethanol showing higher extraction potential compared to others. The effectiveness of the solvent in extraction is influenced by diverse parameters like conditions, solvent type and extraction techniques (35).

3.4.2. TPC and TFC

Various studies have demonstrated the significant contribution of TPC and TFC to the overall antioxidant capacity of fruits [30]. It is noted that different plants exhibit diverse properties against various parameters, owing to the presence of different phytochemicals essential for biological functions. Table 2 presents the TPC and TFC extracted from *W. coagulans* fruits using different solvents. Notably, the highest concentration of TPC (499 ± 0.64 GAE per 100g of dry sample) and TFC (310 ± 0.07 CE per 100g) was observed with aqueous ethanol, while distilled water extracts show the lowest TPC and TFC, ranging from 338 ± 0.32 GAE and 189 ± 0.01 CE per 100g of dry sample, respectively. The extraction efficiency varies significantly (p<0.05) among the tested solvents, indicating their differential ability to extract phenolic constituents from the fruits. The order of phenolic extraction efficiency was aqueous ethanol > aqueous methanol > absolute ethanol > absolute methanol > distilled water. The TFC showed a similar pattern, with aqueous ethanol yielding the highest efficiency, followed by distilled water, aqueous methanol, absolute ethanol and absolute methanol. Solvent polarity, sample composition, and antioxidant affinity are some of the factors that determine a solvent's capacity to extract bioactive chemicals [36]. Variations in TPC and TFC of *W. coagulans* fruits may also be affected by various factors like soil characteristics and growth conditions, which influence phytochemical accumulation. The present findings demonstrated enhanced phenolic and flavonoid recovery compared with previously reported studies (35).

3.4.3. Antioxidant activity in linoleic acid systems

Linoleic acid undergoes oxidation, leading to the formation of peroxides. These peroxides oxidize Fe^{2+} to Fe^{3+}, which subsequently forms a complex with thiocyanate ions (SCN^-). A higher concentration of peroxides during the reaction results in increased absorbance. This elevated absorbance signifies a lower antioxidant potential and a stronger antioxidant capacity due to the abundance of peroxides. By assessing the antioxidant capacity, the efficacy of plant extracts from *W. coagulans* inhibiting lipid peroxidation was shown in Table 2. The inhibition level for linoleic acid oxidation is as follows: 67% and 73% for absolute and aqueous methanol, 70% and 80% for absolute and aqueous ethanol and 53% for distilled water. Plant extracts extracted with aqueous ethanol exhibited considerably better peroxidation inhibition as compared to other extracts (P < 0.05), attributed to their higher overall phenolic content. All investigated samples exhibit considerably reduced oxidant activity (P < 0.05) than BHT (92.01%) when *W. coagulans* fruit extract is mixed with synthetic antioxidants (BHT), suggesting that BHT is less effective at inhibiting linoleic acid oxidation. The order in which *W. coagulans* fruit extracts inhibited linoleic acid peroxidation was aqueous ethanol > aqueous methanol > absolute ethanol > absolute methanol > distilled water.

3.4.4. DPPH radical scavenging assay

The antioxidant capacity of various materials, such as natural extracts and refined chemicals, is frequently evaluated using the DPPH radical scavenging method. Because of its delocalized electrons, DPPH is a persistent free radical that has a purple hue and it shows absorption at 517 nm. The transformation of the DPPH radical to its reduced form occurs when it interacts with an antioxidant capable of donating a proton. This reaction results in the change of color from purple to yellow in the solution. The alteration is a consequence of the electron from the DPPH radical pairing with the hydrogen atom from the antioxidant, leading to the formation of the reduced DPPH species [37,38]. The DPPH radical scavenging capacity (in terms of percentage inhibition) of the extracts using a variety of solvent systems is shown in Table 1. The *W. coagulans* extract expressed radical scavenging activity with an IC_{50} value within the range of 9.27-16.52 μg/mL. The extract in aqueous ethanol shows a 9.27 μg/mL, which is the least IC_{50} value that shows the prominent free radical scavenging activity, while the extract in distilled water is 16.52 μg/mL, which is the highest IC_{50} value and shows the least amount of free radical scavenging activity. The order of the free radical scavenging effectiveness was aqueous ethanol > aqueous methanol > absolute ethanol > absolute methanol > distilled water, according to the results from different extraction solvents. The extracts showed statistically significant differences ($P < 0.05$). Additionally, the current study's DPPH scavenging activity was higher than previously documented values [35].

3.5. A comparative analysis of PCA and antioxidant activity

A comparison with recent plant-mediated metal oxide nanomaterials clearly demonstrates that particle size and phytochemical richness of the extract are decisive factors governing antioxidant and photocatalytic performance. Studies by Kolotygina et al. and Adraoui et al. [40,24] established a strong correlation between extract antioxidant activity, reduced NP size and enhanced photocatalytic efficiency. In line with this trend, the *W. coagulans*-mediated ZnO NPs synthesized in the present work exhibit a notably small crystallite size (~9.25 nm), which is smaller than many reported green-synthesized ZnO systems, particularly those derived from fruit peels and agricultural wastes. Compared with larger ZnO particles (≈170–192 nm) that require higher catalyst loading or process optimization to achieve complete dye degradation, the present ZnO NPs achieve ~90% degradation under natural solar irradiation without complex optimization strategies. This enhanced performance is attributed to (i) efficient bio-capping by phenolics and flavonoids, (ii) improved charge separation, and (iii) increased surface-to-volume ratio that promotes reactive oxygen species generation. Moreover, unlike many reports that focus solely on photocatalysis, the present study integrates antioxidant profiling (TPC, TFC, DPPH, lipid peroxidation inhibition) with photocatalytic performance, offering mechanistic insight into how extract chemistry influences NP functionality. This dual antioxidant–photocatalytic evaluation highlights a clear advantage of *W. coagulans* fruit extract as a multifunctional green precursor, positioning the present work as a balanced advancement over existing literature for environmentally benign ZnO nanomaterials with relevance to both environmental remediation and biomedical applications. Table 1. Comparative overview of plant-mediated zinc oxide and other metal oxide NPs, highlighting particle size, antioxidant potential and photocatalytic performance.

Table 1. Comparative overview of plant-mediated zinc oxide and other metal oxide NPs, highlighting particle size, antioxidant potential and photocatalytic performance.

Plant source/material	Nano material	Particle/crystallite size	Target pollutant/activity	Photocatalytic efficiency	Key remarks	Reference
W. coagulans fruit extract	ZnO	~9.25 nm	Phenol red dye (solar light)	~90% in 240 min	Very small crystallite size; strong bio-capping; high	This wor

					antioxidant activity (TPC, TFC, DPPH)	k
Diospyros kaki peel	ZnO	~192 nm	Methylene blue	100% in 270 min	Larger particle size; activity optimized via Box–Behnken design	[39]
Sea buckthorn extract	ZnO	~13 nm	Methylene blue (UV)	96.4%	The high antioxidant activity of the extract led to a smaller size and higher photocatalysis.	[40]
E. alata leaf extract	ZnO	5–30 nm	Methylene blue	87% in 90 min	Moderate activity; higher band gap (3.3 eV)	[41]
Papaya peel extract	ZnO	~170 nm	Rhodamine B (sunlight)	Significant degradation	Larger particles; multifunctional bioactivity	[42]
R. damascena waste extract	ZnO	nanoscale	Orange G dye (sunlight)	Enhanced degradation	Size optimization crucial for activity	[24]
C. proximus extract	TiO_2	~4 nm	RhB dye	97% in 50 h	Excellent crystallinity; slower kinetics	[43]
P. longifolia leaf extract	CuO	Nanoscale	RhB dye	90.5% in 80 min	Multifunctional photocatalytic & antifungal	[44]

Table 2. Extract yield, TPC, TFC, DPPH and % inhibition of *W. coagulans fruit* extract.

Solvents	Yield (%)	TPC GAE (mg/100g)	TFC CE (mg/100g)	Inhibition of linoleic acid (%)	IC_{50} values (μg/mL)
Absolute methanol	7.21±0.1	386±0.82	232±0.02	67.5±0.27	13.95±0.05
Absolute ethanol	8.60±0.14	438±0.39	267±0.03	70.61±0.42	12.05±0.08
Aqueous methanol	9.32±0.17	454±0.79	278±0.06	73.52±0.61	10.55±0.02
Aqueous ethanol	10.21±0.20	499±0.64	310±0.07	80.40±0.41	08.27±0.07
Distilled water	6.06±0.05	338±0.32	189±0.01	53.20±0.34	16.52±0.06

Three replicates were used to determine the mean ± SD values.

4. Conclusion

W. coagulans fruit extract was used as a reducing and stabilizing agent to prepare the ZnO NPs using an eco-friendly approach, which provides controlled NP synthesis without using hazardous reagents. The XRD, SEM, FTIR and UV–visible techniques were used to characterize the prepared NPs. ZnO NP production was confirmed by a distinctive absorption band at 365 nm, while XRD patterns revealed a hexagonal wurtzite crystalline phase with an average crystallite size of almost 9.25 nm. Morphological analysis revealed irregularly shaped particles with aggregate formation, while FTIR spectra displayed Zn–O vibrational bands around 582 cm^{-1} together with bioactive functional groups originating from plant metabolites, confirming effective surface functionalization. The antioxidant activity (AOA) of *W. coagulans* fruit extracts was investigated using TPC, TFC, linoleic acid oxidation inhibition and DPPH radical scavenging assays, with aqueous ethanol extracts showing the strongest AOA response. Furthermore, the

photocatalytic performance of the ZnO NPs was evaluated through phenol red degradation under sunlight exposure, achieving nearly 90% removal within 240 minutes. This enhanced activity is attributed to efficient charge carrier separation and reactive oxygen species generation, promoting oxidative mineralization of dye molecules into harmless end products. The present study demonstrates a sustainable route for preparing ZnO NPs with notable AOA and photocatalytic properties. The findings highlight the potential of *W. coagulans*-mediated ZnO NPs as multifunctional nanomaterials for environmental remediation and applications in biomedical fields. Future studies should focus on tuning particle size and optimization of photocatalytic parameters, along with *in vitro* and *in vivo* biosafety analysis of the ZnO NPs prepared using *W. coagulans* extract.

Acknowledgment: The authors extend their appreciation to the Deanship of Scientific Research and Libraries in Princess Nourah bint Abdulrahman University for funding this research work through the Research Group project, Grant No. (RG-1445-0041).

Availability of Data and Materials: The datasets used and analyzed during the current study are available from the corresponding author on reasonable request.

Funding: This research was funded by the Deanship of Scientific Research and Libraries in Princess Nourah bint Abdulrahman University through the Research Group project (Grant No. RG-1445-0041).

Author Contributions: MI, NA, AHA, NT, AN conceived and designed the research framework; **MMA, MSA, MA** carried out the experimental and computational work; **MA, IB, AHA, AN** provided critical guidance on the analytical methods and interpretation of results; **NA, MA, IB, NT** performed the data analysis; **MMA, MSA, MI** prepared the initial draft of the manuscript. All authors have read and approved the final manuscript. All authors contributed to editorial changes in the manuscript. All authors have participated sufficiently in the work and agreed to be accountable for all aspects of the work.

Conflicts of Interest: The authors declare no conflict of interest.

References

1. Lu, X.Y. Synthesis of Nano-Co_3O_4-Based Electrocatalysts and Their Performance in Direct Methanol Fuel Cells. *Journal of Ovonic Research* 2025, 21(6), 675–691. https://doi.org/10.15251/JOR.2025.216.675
2. Ibrahim, K.M.; Saleh, W.R.; Taradh, A.Y. Tuning Optical Properties of ZnO Nanorods Through Doping with Au, Cu, Pt, Ni, and Gr Nanoparticles. *Journal of Ovonic Research* 2025, 21(6), 761–768. https://doi.org/10.15251/JOR.2025.216.761
3. Nazir, A., Akbar, A., Baghdadi, H.B., ur Rehman, S., Al-Abbad, E., Fatima, M., Iqbal, M., Tamam, N., Alwadai, N., Abbas, M. Zinc oxide nanoparticles fabrication using Eriobotrya japonica leaves extract: Photocatalytic performance and antibacterial activity evaluation. *Arabian Journal of Chemistry* 2021, 14, 103251. https://doi.org/10.1016/j.arabjc.2021.103251
4. Sangeetha, G.; Rajeshwari, S.; Venckatesh, R. Green Synthesis of Zinc Oxide Nanoparticles by Aloe barbadensis Miller Leaf Extract: Structure and Optical Properties. *Materials Research Bulletin* 2011, 46, 2560–2566. https://doi.org/10.1016/j.materresbull.2011.07.046
5. Rahman, R.A.; Hua, C.C.; Masdor, N.A. Green Synthesis and Characterization of Zinc Oxide Nanoparticles Using Aloe Vera Leaf Extract. In *The Proceedings of the 1st International Conference of Chemical Science, Engineering and Technology* 2023, 2703(1), 120006. AIP Publishing. https://doi.org/10.1063/5.0115328
6. Happy, A.; Soumya, M.; Kumar, S.V.; Rajeshkumar, S.; Sheba, R.D.; Lakshmi, T.; Nallaswamy, V.D. Phyto-assisted synthesis of zinc oxide nanoparticles using *Cassia alata* and its antibacterial activity against *Escherichia coli*. *Biochemistry and Biophysics Reports* 2019, 17, 208–211. https://doi.org/10.1016/j.bbrep.2019.01.002
7. Hossain, A.; Abdallah, Y.; Ali, M.A.; Masum, M.M.I.; Li, B.; Sun, G.; An, Q. Lemon-fruit-based green synthesis of zinc oxide nanoparticles and titanium dioxide nanoparticles against soft rot bacterial pathogen Dickeya dadantii. *Biomolecules* 2019, 9(12), 9, 863. https://doi.org/10.3390/biom9120863

8. Pestovsky, Y.S.; Martínez-Antonio, A. The Use of Nanoparticles and Nanoformulations in Agriculture. *Journal of Nanoscience and Nanotechnology* 2017, 17(12), 8699–8730. https://doi.org/10.1166/jnn.2017.15041
9. Ismail, I.; Balachandran, S.; Devi, M.G. Synthesis, characterization and application of nanoparticles in wastewater treatment. *Indian Chemical Engineer* 2019, 61(1), 77–86. https://doi.org/10.1080/00194506.2018.1469099
10. Davar, F.; Majedi, A.; Mirzaei, A. Green Synthesis of ZnO Nanoparticles and Its Application in the Degradation of Some Dyes. *Journal of the American Ceramic Society* 2015, 98(6), 1739–1746. https://doi.org/10.1111/jace.13467
11. Sohail, M.F.; Rehman, M.; Hussain, S.Z.; Huma, Z.; Shahnaz, G.; Qureshi, O.S.; et al. Green Synthesis of Zinc Oxide Nanoparticles by Neem Extract as Multi-Facet Therapeutic Agents. *Journal of Drug Delivery Science and Technology* 2020, 59, 101911. https://doi.org/10.1016/j.jddst.2020.101911
12. Aldalbahi, A.; Alterary, S.; Almoghim, R.A.A.; Awad, M.A.; Aldosari, N.S.; Alghannam, S.F.; et al. Greener Synthesis of Zinc Oxide Nanoparticles: Characterization and Multifaceted Applications. *Molecules* 2020, 25(18), 4198. https://doi.org/10.3390/molecules25184198
13. Salem, N.M.; Awwad, A.M. Green synthesis and characterization of ZnO nanoparticles using Solanum rantonnetii leaves aqueous extract and antifungal activity evaluation. *Chemistry International* 2022, 8(1), 12–17.
14. Agarwal, H.; Venkat Kumar, S.; Rajeshkumar, S. A review on green synthesis of zinc oxide nanoparticles – An eco-friendly approach. *Resource-Efficient Technologies* 2017, 3(4), 406–413. https://doi.org/10.1016/j.reffit.2017.03.002
15. Ishwarya, R.; Vaseeharan, B.; Kalyani, S.; Banumathi, B.; Govindarajan, M.; Alharbi, N.S.; Kadaikunnan, S.; Al-anbr, M.N.; Khaled, J.M.; Benelli, G. Facile green synthesis of zinc oxide nanoparticles using Ulva lactuca seaweed extract and evaluation of their photocatalytic, antibiofilm and insecticidal activity. *Journal of Photochemistry and Photobiology B: Biology* 2018, 178, 249–258. https://doi.org/10.1016/j.jphotobiol.2017.11.006
16. Chen, L.; Batjikh, I.; Hurh, J.; Han, Y.; Huo, Y.; Ali, H.; Li, J.F.; Rupa, E.J.; Ahn, J.C.; Mathiyalagan, R.; Yang, D.C. Green synthesis of zinc oxide nanoparticles from root extract of Scutellaria baicalensis and its photocatalytic degradation activity using methylene blue. *Optik* 2019, 184, 324–329. https://doi.org/10.1016/j.ijleo.2019.03.051
17. Adraoui, I.; Saffaj, N.; Mamouni, R.; Jadoualia, S.M. Optimization of Green Synthesis of Zinc Oxide Nanoparticles Using Rosa damascena Residue via Box-Behnken Design and Assessment of their Environmental Activity. *Letters in Applied NanoBioScience* 2025, 14, 174. https://doi.org/10.33263/LIANBS143.174
18. Sadiq, H.; Sher, F.; Sehar, S.; Lima, E.C.; Zhang, S.; Iqbal, H.M.N.; Zafar, F.; Nuhanović, M. Green synthesis of ZnO nanoparticles from Syzygium cumini leaves extract with robust photocatalysis applications. *Journal of Molecular Liquids* 2021, 335, 116567. https://doi.org/10.1016/j.molliq.2021.116567
19. Sone, B.T.; Diallo, A.; Fuku, X.G.; Gurib-Fakim, A.; Maaza, M. Biosynthesized CuO nano-platelets: Physical properties & enhanced thermal conductivity nanofluidics. *Arabian Journal of Chemistry* 2020, 13(1), 160–170. https://doi.org/10.1016/j.arabjc.2017.03.004
20. Iqbal, M.; Shar, G.A.; Ibrahim, S.M.; Iftikhar, S.; Asif, M.; Khan, M.I.; Kusuma, H.S.; Yaseen, M.; Nazir, A. Synthesis and characterization of heterostructured nanoparticle for efficient photocatalytic performance for dye degradation. *Zeitschrift für Physikalische Chemie* 2021, 235(9), 1209–1226. https://doi.org/10.1515/zpch-2019-1562.
21. Salehi, M.; Aghamaali, M.R.; Sajedi, R.H.; Asghari, S.M.; Jorjani, E. Purification and characterization of a milk-clotting aspartic protease from Withania coagulans fruit. *International Journal of Biological Macromolecules* 2017, 98, 847–854. https://doi.org/10.1016/j.ijbiomac.2017.02.034
22. Gupta, V.; Keshari, B. B. Withania coagulans Dunal (paneer doda): A review. *International Journal of Ayurvedic and Herbal Medicine* 2013, 3(5), 1330-1336. https://www.dodaberry.com/wp-content/uploads/2015/10/Ayur-Journal.pdf
23. Mathur, D.; Agrawal, R.C.; Shrivastava, V. Phytochemical screening and determination of antioxidant potential of fruits extracts of Withania coagulans. *Recent Research in Science and Technology* 2011, 3, 26-29.
24. Adraoui, I.; Mamouni, R.; Saffaj, N.; Achemchem, F. Eco-friendly synthesis of zinc oxide nanoparticles using saffron extract and their photocatalytic and antibacterial activities. *Journal of Materials Research* 2023, 38(11), 2874–2884. https://doi.org/10.1557/s43578-023-01024-7.
25. Osuntokun, J.; Onwudiwe, D.C.; Ebenso, E.E. Green synthesis of ZnO nanoparticles using aqueous Brassica oleracea L. var. italica and the photocatalytic activity. *Green Chemistry Letters and Reviews* 2019, 12(4), 444–457. https://doi.org/10.1080/17518253.2019.1687761.
26. Ahmad, N.; Zuo, Y.; Anwar, F.; Abbas, A.; Shahid, M.; Hassan, A.A.; Bilal, M.; Rasheed, T. Ultrasonic-assisted

extraction as a green route for hydrolysis of bound phenolics in selected wild fruits: Detection and systematic characterization using GC–MS–TIC method. *Process Biochemistry* 2021, 111, 79–85. https://doi.org/10.1016/j.procbio.2021.10.021.
27. Ahmad, N.; Anwar, F.; Zuo, Y.; Aslam, F.; Shahid, M.; Abbas, A.; Farhat, L.B.; Al-Mijalli, S.H.; Iqbal, M. Wild olive fruits: Phenolics profiling, antioxidants, antimicrobial, thrombolytic and haemolytic activities. *Arabian Journal of Chemistry* 2022, 15, 104241. https://doi.org/10.1016/j.arabjc.2022.104241.
28. Ahmad, N.; Anwar, F.; Hameed, S.; Boyce, M.C. Antioxidant and antimicrobial attributes of different solvent extracts from leaves and flowers of akk [Calotropis procera (Ait.) Ait. F.)]. *Journal of Medicinal Plants Research* 2011, 5(19), 4879–4887. https://doi.org/10.5897/JMPR.9000211.
29. Selim, Y.A.; Azb, M.A.; Ragab, I.; Abd El-Azim, M.H.M. Green Synthesis of Zinc Oxide Nanoparticles Using Aqueous Extract of Deverra tortuosa and their Cytotoxic Activities. *Scientific Reports* 2020, 10, 3445. https://doi.org/10.1038/s41598-020-60541-1.
30. Ainsworth, E.A.; Gillespie, K.M. Estimation of total phenolic content and other oxidation substrates in plant tissues using Folin–Ciocalteu reagent. *Nature Protocols* 2007, 2, 875–877. https://doi.org/10.1038/nprot.2007.102.
31. Tepe, B.; Daferera, D.; Sokmen, A.; Sokmen, M.; Polissiou, M. Antimicrobial and antioxidant activities of the essential oil and various extracts of Salvia tomentosa Miller (Lamiaceae). *Food Chemistry* 2005, 90, 333–340. https://doi.org/10.1016/j.foodchem.2003.09.013.
32. Moghaddas, S.M.T.H.; Elahi, B.; Darroudi, M.; Javanbakht, V. Green synthesis of hexagonal-shaped zinc oxide nanosheets using mucilage from flaxseed for removal of methylene blue from aqueous solution. *Journal of Molecular Liquids* 2019, 296, 111834. https://doi.org/10.1016/j.molliq.2019.111834.
33. Siripireddy, B.; Mandal, B.K. Facile green synthesis of zinc oxide nanoparticles by Eucalyptus globulus and their photocatalytic and antioxidant activity. *Advanced Powder Technology* 2017, 28(3), 785–797. https://doi.org/10.1016/j.apt.2016.11.026.
34. Joel, C.; Badhusha, M.S.M. Green synthesis of ZnO Nanoparticles using Phyllanthus embilica Stem extract and their Antibacterial activity. *Der Pharmacia Lettre* 2016, 8, 218-223.
35. Ahmad, N.; Arslan, M.; Kashif, A.R.; Abbas, A. Nutraceutical and biological attributes of wild Withania coagulans fruits. *Chemistry International* 2022, 8(3), 106-113. https://doi.org/10.5281/zenodo.7196794.
36. Kamaruddin, H.S.; Megawati, M.; Nurliana, N.; Sabandar, C.W. Chemical Constituents and Antioxidant Activity of Melothria scabra Naudin Fruits. *Borneo Journal of Pharmacy* 2021, 4, 2890. https://doi.org/10.33084/bjop.v4i4.2890.
37. Hasan, M.R.; Haque, M.M.; Hoque, M.A.; Sultana, S.; Rahman, M.M.; Shaikh, M.A.A.; Sarker, M.K.U. Antioxidant activity study and GC-MS profiling of Camellia sinensis Linn. *Heliyon* 2024, 10(1), e23514. https://doi.org/10.1016/j.heliyon.2023.e23514.
38. Abbas, M.; Mumtaz, A.; Alwadai, N.; Iqbal, M.; Nazir, A.; Bibi, I.; Ali, A.; Ahmad, N.; Al Huwayz, M. Ag Nanoparticle Green Synthesis using Litchi chinensis Peels Extract: Mutagenicity, Cytotoxicity, Antimicrobial and Antioxidant Activities Evaluation. *Journal of the Chemical Society of Pakistan* 2026, 48, 59-73.
39. Turkoglu, S.; Kepekçi, R.A.; Keskinkan, O. Photocatalysis of methylene blue by ZnO nanoparticles produced by green synthesis. *International Journal of Phytoremediation* 2026, 28(3), 513–523. https://doi.org/10.1080/15226514.2025.2574902.
40. Kolotygina, V.Y.; Zhilyakov, A.Y.; Bukharinova, M.A.; Khamzina, E.I.; Stozhko, N.Y. Green Synthesis of ZnO Nanoparticles: Effect of Synthesis Conditions on Their Size and Photocatalytic Activity. *ChemEngineering* 2026, 10, 15. https://doi.org/10.3390/chemengineering10010015.
41. Ahmad, S.; Ahmad, S.; Xu, Q.; Khan, I.; Cao, X.; Yang, R.; Yan, H. Green synthesis of gold and silver nanoparticles using crude extract of Aconitum violaceum and evaluation of their antibacterial, antioxidant and photocatalytic activities. *Frontiers in Bioengineering and Biotechnology* 2024, 11, 1320739. https://doi.org/10.3389/fbioe.2023.1320739.
42. Easmin, S.; Bhattacharyya, M.; Pal, K.; Das, P.; Sahu, R.; Nandi, G.; Dewanjee, S.; Paul, P.; Haydar, M.S.; Roy, S.; Dua, T.K. Papaya peel extract-mediated green synthesis of zinc oxide nanoparticles and determination of their antioxidant, antibacterial, and photocatalytic properties. *Bioprocess and Biosystems Engineering* 2024, 47, 65–74. https://doi.org/10.1007/s00449-023-02945-7.
43. Awad, M.A.; Ortashi, K.M.O.; Alenazi, W.; Alfaifi, F.S.; Al-Huqail, A.A. Green Synthesis of Titanium Dioxide

Nanoparticles: Characterization and Evaluation of Their Potential for Photocatalytic and Dielectric Applications. *Molecules* 2025, 30, 4701. https://doi.org/10.3390/molecules30244701.
44. Khan, A.; Guo, Z.; Patil, B.R.; Jiang, Y.; Ahmad, I.; Hu, A.; Khadrawy, S.M. Mechanistic insights into antifungal and photocatalytic efficacy of green synthesized copper oxide nanoparticles: Experimental validation coupled with in silico modelling. *Environmental Technology & Innovation* 2026, 41, 104816. https://doi.org/10.1016/j.eti.2026.104816.